Summer 2023

Static I-V Curve and Aging Test for PIM Characterization in Metallic Contacts

Kalkidan Anjajo
Missouri University of Science and Technology

Department:

STATIC I-V CURVE AND AGING TEST FOR PIM CHARACTERIZATION IN METALLIC CONTACTS

by

KALKIDAN WOLDEMARIAM ANJAJO

A THESIS

Presented to the Graduate Faculty of the

MISSOURI UNIVERSITY OF SCIENCE AND TECHNOLOGY

In Partial Fulfillment of the Requirements for the Degree

MASTER OF SCIENCE IN ELECTRICAL ENGINEERING

2023

Approved by:

Chulsoon Hwang, Advisor
Daryl G. Beetner
Donghyun(Kim) Bill

ABSTRACT

Spring clips and fabric-over-foams (FOFs) are widely used in mobile devices for electrical connection purposes. However, the imperfect metallic connections tend to induce passive intermodulation (PIM), resulting in a receiver sensitivity degradation, known as RF desensitization. Due to the complexity of the PIM characterization, there is not yet a way to evaluate PIM performance using a simple setup for environments like factories. In this study, a current-voltage (I-V) behavior-based PIM evaluation method is proposed and validated with various metallic contacts and contact forces. The test results demonstrated the feasibility of the PIM performance evaluation based on the measured static I-V curve.

After the I-V based PIM estimation, the impact of the aging environment on the level of passive intermodulation (PIM) and DC resistance of nickel-based conductive FOF materials presented. These materials are widely used to maintain metallic connections between modules and chassis in electronic devices. The PIM caused by the loose metallic contact of these materials mainly affects a receiver's RF sensitivity in mobile devices. This aging test under elevated temperature and relative humidity conditions offers an experiment-based approach with respect to various metallic contact cases. Energy dispersive spectroscopy and scanning electron microscopy are used to characterize the change in material composition and the contact surface throughout the aging. The experimental environmental effects showed the aging on the generated PIM level to have little to no impact and DC resistance of these metallic contact materials increased.

ACKNOWLEDGMENTS

I would like to express my deepest gratitude to my advisor, Dr. Chulsoon Hwang, for his invaluable guidance, unwavering support, and continuous encouragement throughout my master's program. His expertise, patience, and dedication have been instrumental in shaping my research and academic journey. I am truly grateful for the opportunities he provided me and the knowledge he imparted. I would also like to extend my heartfelt appreciation to all the faculties in the EMC Lab for their expertise and commitment to excellence in research. Their mentorship and encouragement have played a significant role in my professional growth.

To my family, I am profoundly grateful for their unconditional love, understanding, and constant encouragement. Their unwavering support has been a source of strength during challenging times. In particular, I would like to dedicate this thesis to my beloved mother, who may not be physically present but remains a guiding light in my life. Her memory continues to inspire me, and I am forever grateful for the values and lessons she instilled in me.

I would also like to express my gratitude to my friends, whose friendship and support have made my journey enjoyable and memorable. Finally, I would like to thank all the individuals who have contributed to my research and thesis, whether directly or indirectly. Your insights and feedbacks have enriched my work and expanded my understanding.

TABLE OF CONTENTS

Page

LIST OF ILLUSTRATIONS

LIST OF TABLES

NOMENCLATURE

Symbol	Description
a_n	Polynomial coefficient
ω	Angular frequency
Zs	Source Impedance
Z_L	Load Impedance

1. INTRODUCTION

Passive intermodulation (PIM) is a significant concern in modern communication systems, particularly in wireless networks, where it can degrade signal quality, cause interference, and impact system performance [1]-[3]. PIM refers to the generation of unwanted intermodulation products when high-power signals interact within passive components such as antennas, connectors, cables, and filters. These intermodulation products fall within the desired frequency band, interfering with the primary signals and introducing noise and distortion.

PIM occurs due to non-linearities within passive components, which introduce unwanted intermodulation products. Factors such as metal-to-metal contacts, dissimilar metals, corrosion, loose connections, and manufacturing defects contribute to these non-linearities. As a result, harmonics and intermodulation products are generated within the desired frequency range, leading to degraded signal quality and potential interference.

The effects of PIM include signal degradation, increased noise levels, reduced coverage range, and diminished overall system performance. These unwanted intermodulation products can also cause interference with neighboring communication channels or services, posing challenges in wireless networks where multiple signals coexist.

To detect and measure PIM, specialized testing equipment is employed. PIM analyzers, spectrum analyzers, and vector network analyzers are utilized to generate high-power test signals and analyze intermodulation products. Comprehensive testing is necessary, considering the intermittent nature of PIM and its dependence on system operating conditions [4].

Mitigation techniques for PIM include careful component selection and installation practices. High-quality components with low PIM specifications are preferred to minimize intermodulation. Proper cable management, secure connections, and regular maintenance are crucial in reducing the risk of PIM-related issues.

The significance of PIM in the telecommunications industry cannot be understated. As wireless networks and data transmission continue to evolve and grow in importance, the impact of PIM on system performance and reliability becomes increasingly critical.

Passive intermodulation (PIM) estimation plays a crucial role in electronic devices, particularly in wireless communication systems. Accurate estimation of PIM is essential for ensuring reliable and high-quality signal transmission, optimizing system performance, and complying with industry standards. The importance of PIM estimation can be seen in various aspects of electronic device design, deployment, and maintenance.

Firstly, PIM estimation helps in identifying potential sources of intermodulation distortion and preventing issues in electronic devices. By assessing PIM levels, designers can select components with low PIM characteristics and implement appropriate measures to minimize PIM generation. This proactive approach during the design and manufacturing stages helps in preventing performance degradation and interference in wireless communication systems [5]. Secondly, PIM estimation is vital for optimizing the performance of wireless networks. Intermodulation distortion caused by PIM can lead to reduced coverage range, degraded signal quality, and increased noise levels. By estimating PIM levels, network operators can identify and address potential sources of interference, ensuring efficient spectrum utilization and maximizing network capacity [6].

Thirdly, PIM estimation contributes to delivering a superior user experience in wireless communication. Intermodulation distortion can result in dropped calls, poor voice quality, and reduced data transfer rates. Accurate estimation of PIM levels enables manufacturers and service providers to design and deploy electronic devices that meet performance standards, ensuring reliable and high-quality communication for end-users [7].

Moreover, PIM estimation plays a crucial role in troubleshooting and maintenance of electronic devices and communication systems. In cases of performance issues or interference complaints, PIM estimation helps technicians identify and locate potential sources of intermodulation distortion. This information enables targeted inspections, repairs, or replacements of faulty components, minimizing downtime and optimizing system reliability [8].

Finally, PIM estimation aligns with industry standards and regulations. Regulatory bodies often define maximum acceptable PIM levels to ensure interference-free operation of wireless networks. Accurate estimation of PIM allows manufacturers and operators to ensure compliance with these standards, facilitating the smooth deployment and operation of electronic devices within the regulatory framework [9].

In general, PIM estimation is of paramount importance in electronic devices, particularly in wireless communication systems. It aids in preventing issues, optimizing network performance, enhancing the user experience, facilitating troubleshooting and maintenance, and ensuring compliance with industry standards. By prioritizing PIM estimation, stakeholders can deliver reliable and high-quality wireless communication, meeting the demands of today's interconnected world.

2. LITERATURE REVIEW/BACKGROUND

2.1. PIM IN RF CONNECTORS

The paper in [10] addresses the issue of passive intermodulation (PIM) in coaxial connectors and specifically investigates the impact of contact pressure on PIM generation. Passive intermodulation is a phenomenon where unwanted signals are generated at different frequencies due to nonlinearities in the system. It can degrade the performance of RF systems, particularly in high-power and wideband applications.

It introduced the importance of coaxial connectors in RF systems and the significance of understanding PIM in such connectors and highlighted that the contact pressure between the center and outer conductors in coaxial connectors is a critical parameter affecting the electrical performance and reliability of the connectors.

The study employs a comprehensive experimental setup to investigate the relationship between contact pressure and PIM levels in coaxial connectors. It uses two different types of coaxial connectors and varies the contact pressure between them to observe its impact on PIM generation. The PIM levels are measured using a specialized PIM test system.

The experimental results in Figure 2.1 demonstrate a clear correlation between contact pressure and PIM levels. The authors find that increasing the contact pressure leads to a reduction in PIM, indicating that proper contact pressure is crucial for minimizing PIM in coaxial connectors. They attribute this behavior to the improvement in electrical contact and reduced resistance at the contact interface.

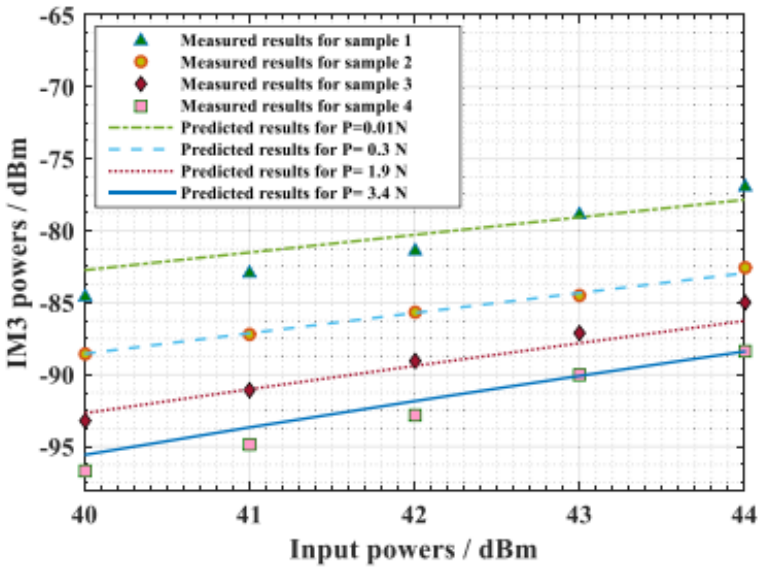

Figure 2.1 Comparisons of the Predicted and Measured Results for Connector Samples with Different Contact Pressures. Source: Q. Jin[10].

Furthermore, the paper discusses the impact of contact pressure on the connector's electrical characteristics such as return loss and insertion loss. It reveals that as contact pressure increases, both return loss and insertion loss improve, which further supports the importance of proper contact pressure for optimal connector performance.

Overall, the study highlights the significance of contact pressure in coaxial connectors and its direct influence on passive intermodulation. It emphasizes the need for careful consideration of contact pressure during connector installation and maintenance to minimize PIM and ensure reliable RF system operation. The findings of this research provide valuable insights for connector manufacturers, system designers, and operators in mitigating PIM-related issues in RF systems.

Another work done regarding Prediction of PIM from coaxial connectors in microwave networks demonstrates that PIM is a critical concern in microwave networks

as it can cause interference and degrade system performance. This paper focuses on predicting passive intermodulation specifically arising from coaxial connectors in microwave networks. It aims to develop a model that accurately estimates the level of PIM generated by these connectors.

The paper provides an overview of passive intermodulation and its significance in microwave systems. It highlights those connectors, which are essential components in microwave networks, can introduce PIM due to nonlinear behavior caused by mechanical imperfections, material properties, and junction effects.

To predict the PIM levels generated by coaxial connectors, it proposes a mathematical model based on the concept of nonlinear junctions. The model takes into account various factors such as contact resistance, junction asymmetry, and the presence of dissimilar metals. It utilizes circuit theory and considers the nonlinear behavior of the connector to estimate the PIM levels.

To validate the proposed model, experiments are conducted using a variety of coaxial connectors. The PIM levels generated by these connectors are measured and compared the results with the predictions obtained from the model. The experimental data is used to verify the accuracy and reliability of the model in estimating PIM levels.

The results in Figure 2.2 demonstrate that the proposed model provides accurate predictions of PIM levels in coaxial connectors. A good correlation has been found between the measured PIM levels and the values estimated by the model. This indicates that the model can be used as a predictive tool to assess the PIM performance of coaxial connectors in microwave networks.

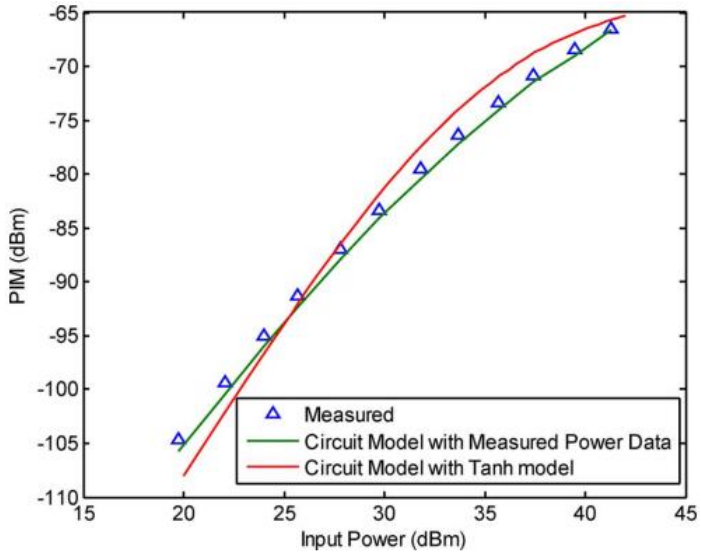

Figure 2.2 PIM Versus Input Power. Source: J. Henrie [11].

Overall, the paper presents a mathematical model for predicting passive intermodulation levels arising from coaxial connectors in microwave networks. The model takes into account various factors that contribute to PIM generation and provides accurate estimations of PIM levels. This model can be valuable for system designers and engineers in evaluating the performance of coaxial connectors and mitigating potential PIM-related issues in microwave networks.

A study of the PIM induced by nonlinear characteristics of RF Connectors in [12] also demonstrates that PIM is a significant issue in RF systems, particularly in high-frequency applications, as it can degrade system performance and introduce interference. This paper focuses on studying the passive intermodulation induced by the nonlinear characteristics of RF connectors, aiming to gain insights into the underlying mechanisms and improve PIM mitigation strategies.

It begins by providing an overview of passive intermodulation and its impact on RF systems and highlights that RF connectors, due to their inherent nonlinear behavior, can contribute to the generation of PIM signals. This motivates the need for a comprehensive study to understand the nonlinear characteristics of RF connectors and their relationship with PIM.

The study employs an experimental approach to investigate the nonlinear behavior of RF connectors and its influence on PIM generation. Several commonly used RF connectors are selected and subject them to various testing scenarios. It analyzes the connectors' electrical performance, including return loss, insertion loss, and third-order intermodulation distortion (IMD3).

The experimental results in Figure 2.3 reveal the presence of nonlinear characteristics in RF connectors, which contribute to the generation of PIM. The authors identify those factors such as contact resistance, contact material, and mechanical imperfections play significant roles in inducing nonlinear behavior and subsequent PIM. They quantify the relationship between these factors and the level of PIM generated by the connectors. The paper investigates the impact of connector design modifications and material selection on PIM levels. The authors explore different strategies to mitigate PIM, such as optimizing contact interfaces, reducing contact resistance, and improving the mechanical integrity of the connectors. They evaluate the effectiveness of these strategies in reducing PIM and provide insights into their practical implementation.

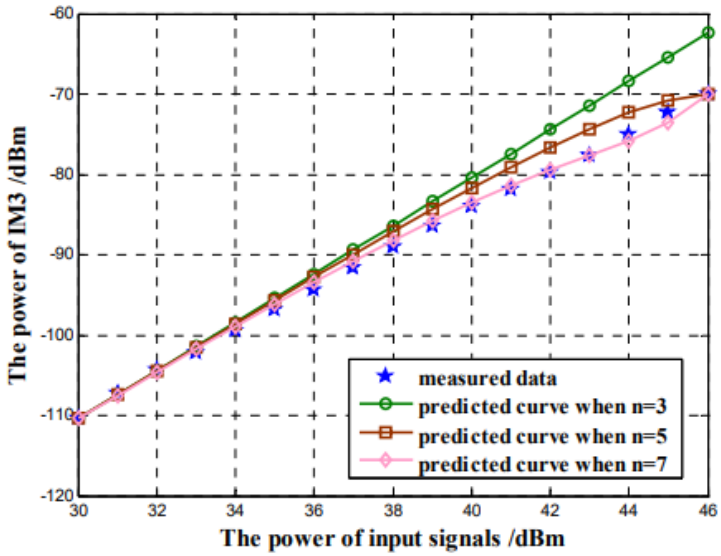

Figure 2.3 Comparison Result of Measured Data and Two Theory Models: 3rd Harmonics Power Dependence on Carrier Power. Source: Q. Jin [12].

The study highlights the nonlinear characteristics of RF connectors and their contribution to passive intermodulation. The findings emphasize the importance of understanding and mitigating PIM in RF systems. The insights gained from this research can aid in the development of improved connector designs, material selection, and optimization techniques to minimize PIM and enhance the performance of RF systems.

2.2. PIM IN MOBILE APPLICATIONS

In mobile devices, the degradation of receiver sensitivity (desensitization) is a significant concern. One of the causes is passive intermodulation (PIM). PIM is challenging to identify, as there are many causes – nonlinear materials, poor metallic contacts, surface oxidation, vibration, etc. [13]. Moreover, the generation mechanisms are complicated–semiconductor, electron-tunneling, electro-thermal, micro discharge, and contact mechanisms [14].

PIM in mobile applications is commonly caused by loose metal contacts. Among the contributing factors to PIM, the corresponding contact level is dominant [14], which models the metallic contacts as a metal-insulator-metal structure with current-dependent nonlinearity. This current-dependent nonlinearity can be modeled as a nonlinear resistor [15]. It has been observed that the PIM can be predicted based on the current voltage (I-V) characteristics of metallic contacts, the study in [16] achieved a good correlation between measured and theoretically calculated PIM under different bias voltages, based on the measured I-V curve of a silicon slice.

Presently, the spring clips and fabric-over-foams (FOFs) provide a good solution allowing number of modules to be assembled in a compact device. At the same time, the spring and FOF contacts tend to cause PIM because the contact junction is not soldered, resulting in RF desensitization if installed with insufficient contact force [17]. The PIM-Force relationship is demonstrated in Figure 2.4.

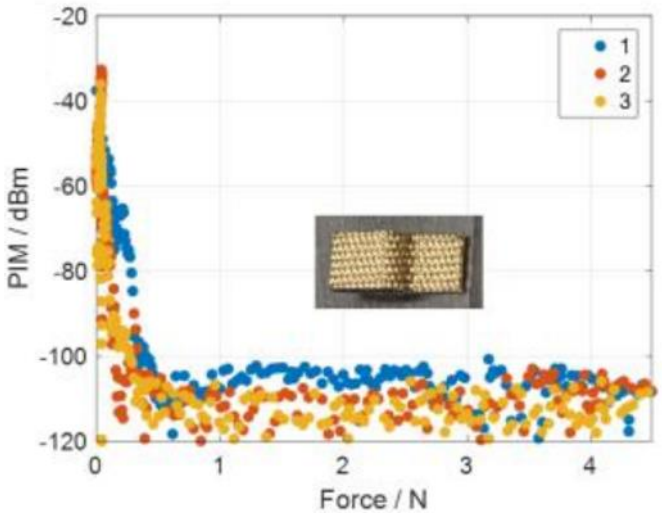

Figure 2.4 FOF Test Data. Source: S. Xia [17].

To characterize the PIM, expensive instruments and microwave devices are needed, such as s signal generator, duplexer, and spectrum analyzer, but usually these instruments are unavailable and inappropriate for large-scale testing in a factory setting. The ability to quantify PIM level in a factory setting would help reduce risk of RF desensitization caused by poor metallic contacts. In [18], a low cost 4 wire DCR measurement was proposed to estimate the contact generated PIM for spring contacts and results are shown in Figure 2.5. However, the drawback for this method was, only the lowest PIM can be estimated but not the level of the PIM itself for each corresponding contact. Therefore, a simple setup to identify PIM risk at each contact is in demand.

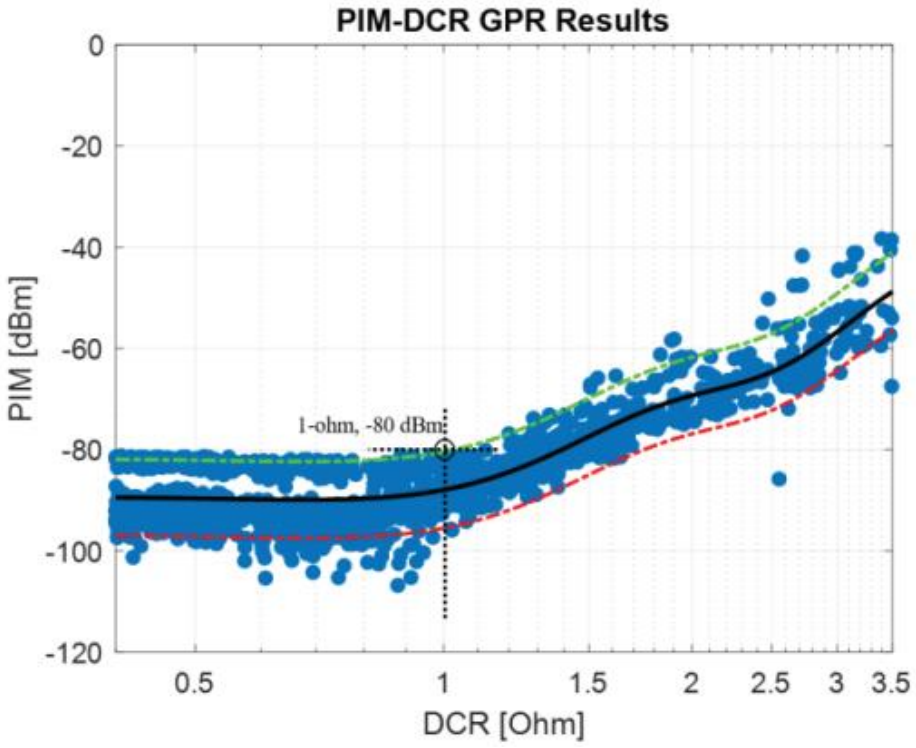

Figure 2.5 GPR Analysis Results for the Measured PIM-DCR Data. Source: S. Xia [18].

3. CHARACTERIZATION AND EXPERIMENTAL PROCEDURE

3.1. MEASUREMENT SYSTEM

3.1.1. Measurement Set-up. A measurement system was built to investigate the correlation between the PIM and I-V, as shown in Figure 3.1. The PIM level measurement setup was adapted from [17].

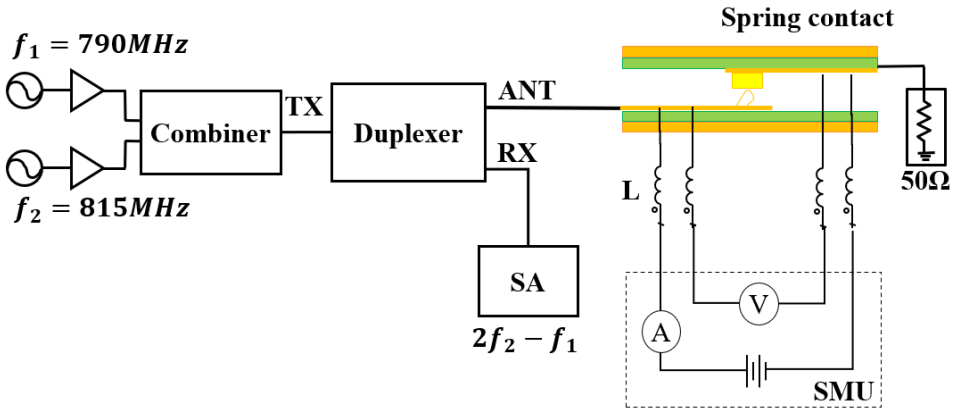

Figure 3.1 PIM-IV Measurement System.

The amplified signals (790 and 815 MHz) are combined and then transmitted to the transmitter port of a low-PIM duplexer - frequency range: 790~821 MHz (Transmitter) and 832~863 MHz (Receiver). At the antenna port of the duplexer, the combined two-tone signal is injected to the DUT – the spring contact or FOF contact. The other end of the DUT is terminated with a high-power and low-PIM 50 Ω load. Only the third order PIM (the highest magnitude compared to other higher order intermodulation products) has been considered and only $2f_2 - f_1$, $(f_2 > f_1)$ is monitored. The induced third order PIM (840MHz) is monitored by the spectrum analyzer (SA), with 10 Hz resolution bandwidth.

A 4-wire resistance measurement setup was implemented to allow accurate static I-V tests with a source measure unit (Keithley 2401). Surface mount inductors were placed to prevent the impact on the RF signal path while conducting I-V tests.

The detailed view of the test fixture for the spring contact is shown in Figure 3.2(a), the spring clip is soldered on the bottom board, and landing pad namely (a piece cut out from an actual phone chassis) is soldered on the top board. The top board is connected to a force gauge with 0.001N resolution. The top board's height is controlled by a step motor of 0.3 μm resolution. According to the S11 and S21 performance [17], by pressing down the top board until there is a good contact, the capacitive coupling between the two boards provides a good enough return path.

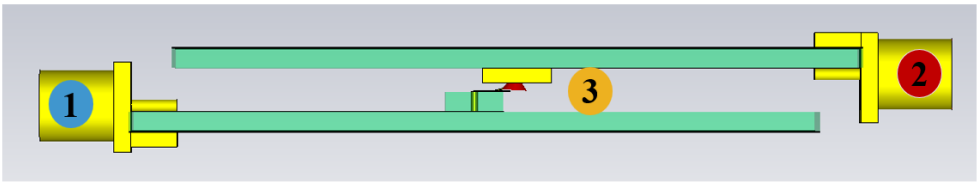

(a)

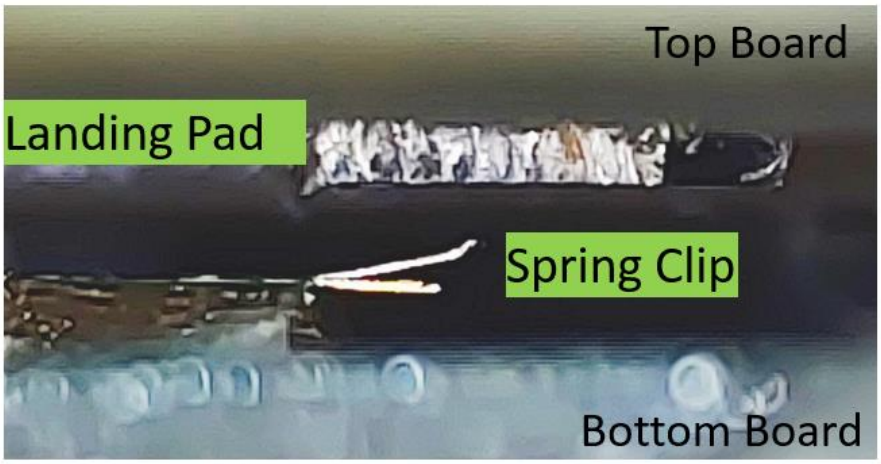

(b)

Figure 3.2 Test Fixture for Spring Contact: (a) Full-Wave Simulation Model, (b) Spring Contact – Spring Clip and Landing Pad.

3.1.2. Measurement Procedure. The signal generators are turned off to disable the PIM measurement, and current is then swept from 10 mA to 150 mA, for both polarities' currents: +10, -10, +16, -16, +22, -22, …, +150, -150 mA as shown in Figure 3.3. Gradually increasing the current amplitude helps to avoid potential high current melting at the tiny contact junction in the beginning.

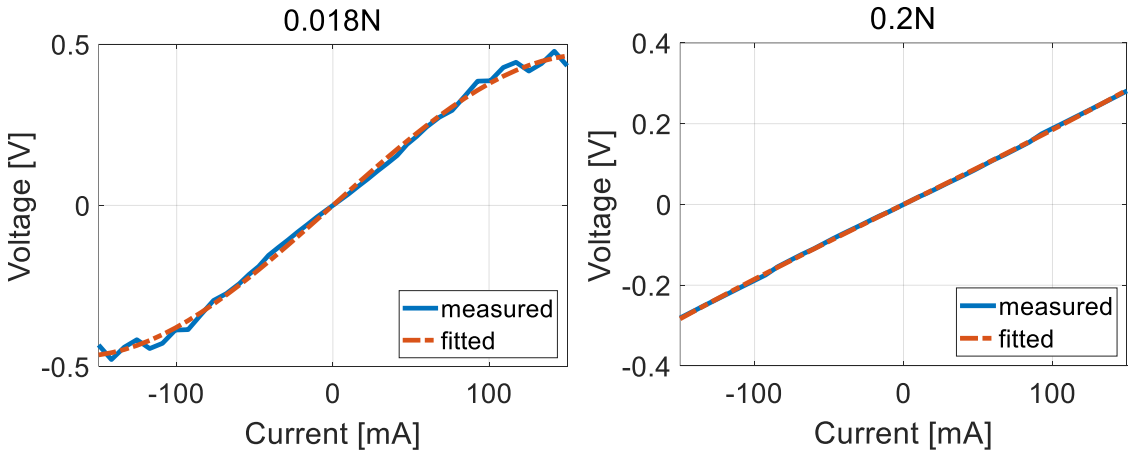

(a) (b)

Figure 3.3 I-V Test Results: (a) I-V Curve at Loose Contact, (b) I-V Curve at Good Contact.

If the negative sweep is processed after finishing the positive sweep, the PIM level may change dramatically. The highest input power used for this work is 20 dBm, while the spring contact resistance is typically several Ohms or lower, and the source and load impedance is 100 Ω in total, so the maximum current is set to be 150 mA. As the input power increases, the current needed likewise increases. For example, if measured to a higher input power such as 30 dBm, then the maximum current needs to be 400 mA. During the measurement of the DC resistance by sweeping the current, the I-V curve of each

contact case could be generated. From Figure 3.4(a), it can be clearly observed in the measured I-V curves that the curves are more non-linear with lower contact force, i.e., loose contact case, and becomes more linear as the contact force increases. Figure 3.4(b) shows the corresponding PIM levels for different contact forces. From the correlation, it can be concluded that the nonlinear coefficient extracted from the I-V curve can be used to represent and characterize the PIM level.

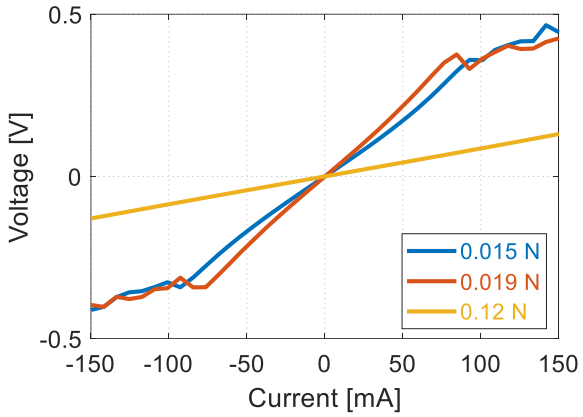

(a)

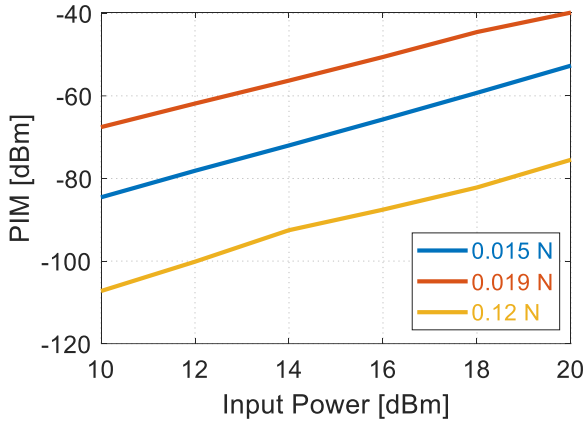

(b)

Figure 3.4 Measurement Results for Spring Clip and Chassis Landing Pad Contact Under Different Contact Forces: (a) I-V Curve, (b) PIM Versus Input Power.

The measured I-V curve is then fitted with a third order polynomial and the polynomial coefficients are extracted. The third order coefficient, a_3, will be used later in this paper to estimate the PIM level at each corresponding contact case.

$$V = a_0 + a_1 I + a_2 I^2 + a_3 I^3 \quad (1)$$

The PIM levels can be checked before and after the I-V tests to ensure that the contact condition has not been changed. Reasonable small differences between pre- and post-PIM the contact junction remains unchanged. It was observed that the I-V sweep can dramatically change the PIM behavior for some loose contacts and the discrepancy between pre- and post-PIM was above 10dB. To ensure the measured I-V curve represents the PIM behavior, only the datasets within 5dB discrepancy between pre- and post-PIM were collected in this paper to demonstrate the relationship between the I-V behavior and the PIM level.

3.2. PIM ESTIMATION

A simplified circuit model of the test fixture with a nonlinear resistor and a 50-ohm load is depicted in Figure 3.5. A nonlinear resistor representing the fitted I-V curve based on (1), is represented as DUT. The PIM level can be estimated based on the V_{f3} (voltage at the PIM frequency which equals $2f_2 - f_1$).

The input current of the I-V block can be expressed as

$$I_{in} = I_{1_{in}} \cdot cos\omega_1 t + I_{2_{in}} \cdot cos\omega_2 t, \quad (2)$$

Then (1) can be represented as

$$V = a_0 + \sum_{n=1}^{3} (a_n {I_{in}}^n) \quad (3)$$

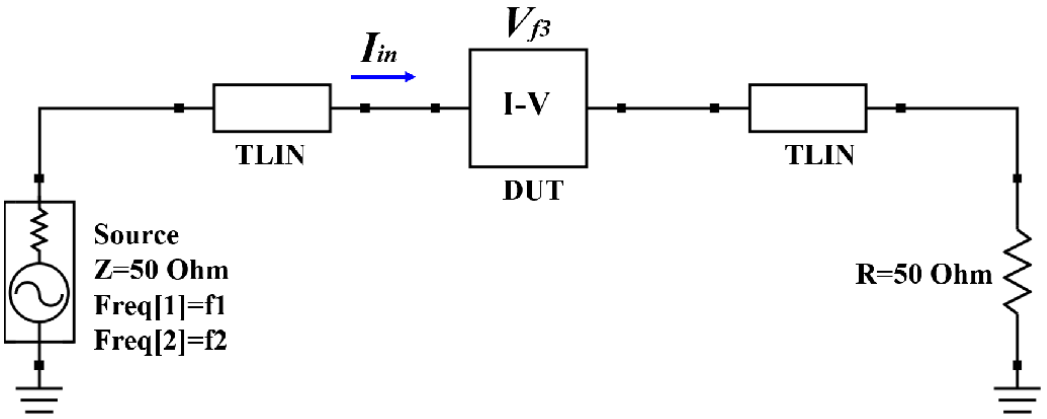

Figure 3.5 Schematics of the Nonlinearity Representation.

The third order PIM component can be extracted (4) and the current can be solved by the cubic equation (5) as follows.

$$V_{f3} = a_3 \frac{3}{4} I_1 I_2^2 \, cos(2\omega_2 - \omega_1)\, t \tag{4}$$

$$a_3 I^3 + a_2 I^2 + (a_1 + Z_s + Z_L) I + (a_0 - V_s) = 0 \tag{5}$$

where Z_S is the 50 Ω source impedance, Z_L the 50 Ω load, and V_S the source voltage. Finally, the PIM can be expressed as

$$PIM_3[dBm] = 20 \cdot log \left| a_3 \frac{3}{4} I_1 I_2^2 \right| + 13.01 \tag{6}$$

The analytic expression of the PIM is verified by comparing the mathematical calculation with the circuit simulation. Based on (6), the relationship between the PIM and the third order coefficient a_3 can be extracted as

$$PIM_3 \propto log_{10}|a_3| \tag{7}$$

An assumption can be made as (8), because the source and load impedance are much higher than the spring contact resistance. As a result, the PIM is only related to the third order coefficient.

$$I_{in1} = I_{in2} \cong \frac{V_s}{2(Z_L+Z_s)} \tag{8}$$

The test fixture's impact is further considered in the estimation process, as shown in Figure 3.6. The 3-port S-parameter block was extracted from the full-wave simulation in representing the test fixture. While this approach can better represent the actual setup, it was found that the simulation results are close enough to the numerical calculation – within 1.5dB. Therefore, the numerical approach (6) is applied in the following estimation process for implementation. The PIM performance of spring and FOF contacts are predicted and compared to measured results in this section.

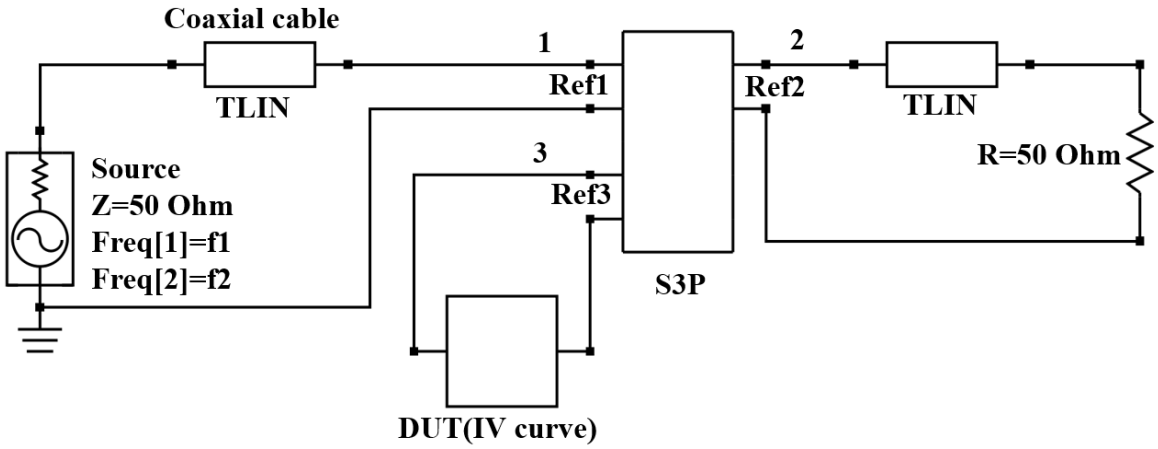

Figure 3.6 PIM Estimation Circuit Schematics Including the Setup Impact.

4. RESULTS AND AGING TEST

4.1. SPRING CONTACTS

In this study, three spring clips shown in Figure 4.1 are used to verify the PIM estimation process. The bottom part of the spring clip is soldered to the bottom PCBs' trace and the curved tip structure on the other end of the spring, contacts the landing pad.

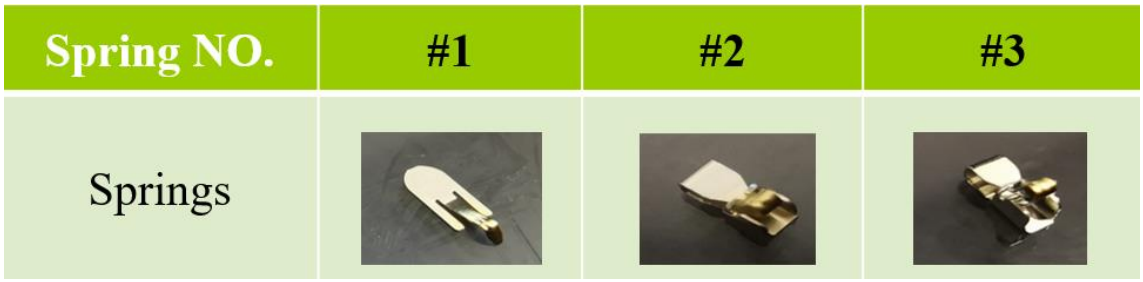

Figure 4.1 Three Types of Characterized Spring Clip.

The measurement and estimation results based on the spring-chassis contact are summarized in Figure 4.2. Note that only the data at 20 dBm input power are shown. Nevertheless, it adequately represents the simulation performance with 10-20 dBm input power because the measured and simulated PIM follow a 3 dB / dB regrowth rate as shown Figure 3.4(b).

The data points that occurred in the high-PIM region (>-60dBm) are due to lose spring contact, which corresponds to stronger nonlinearity. The large discrepancies of the two cases marked in the dashed black block is caused by the self-contact effect [11].

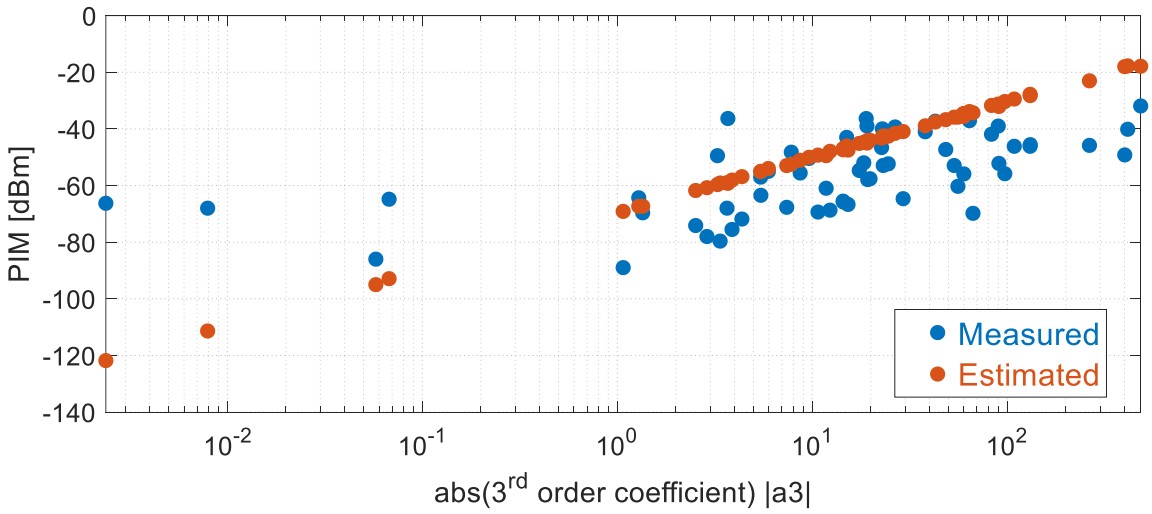

Figure 4.2 Measured and Simulated PIM (at 20 dBm Input Power) Versus Third Order Coefficient (a_3) from the Fitted I-V Curve.

There is already a considerable amount of contact force when the self- contact is made, so the measured I-V curve is much more linear (i.e., the estimated PIM level will be small). On the other hand, the self-contact induces high PIM. As a result, the PIM is much underestimated since the I-V measurement only reveals the main body of the spring clip (of low impedance) instead of the self-contact region. Overall, the simulation captures the trend: the PIM is proportional to the $\log_{10}|a_3|$.

The discrepancy between estimated and measured PIM is summarized in Figure 4.3. There are 120 cases in each group, and for each group, the measured and estimated PIM level is compared with 10-20 dBm input power. More than 96% of cases are captured within 20 dB when compared to measurements.

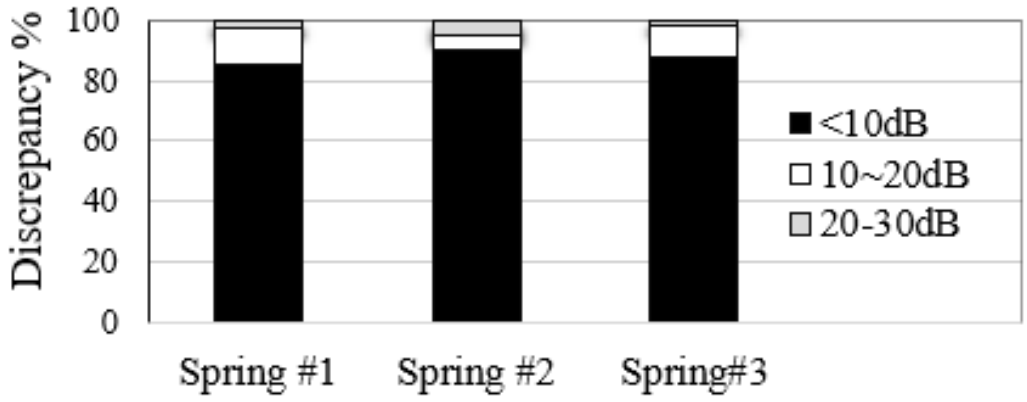

Figure 4.3 Discrepancy of Measured and Simulated PIM for Etched Chassis and Spring Clips.

4.2. FOF CONTACTS

Four types of FOFs shown in Figure 4.4, are tested. The test setup is similar to Figure 3.1. The only difference is that the spring clip is changed to FOF.

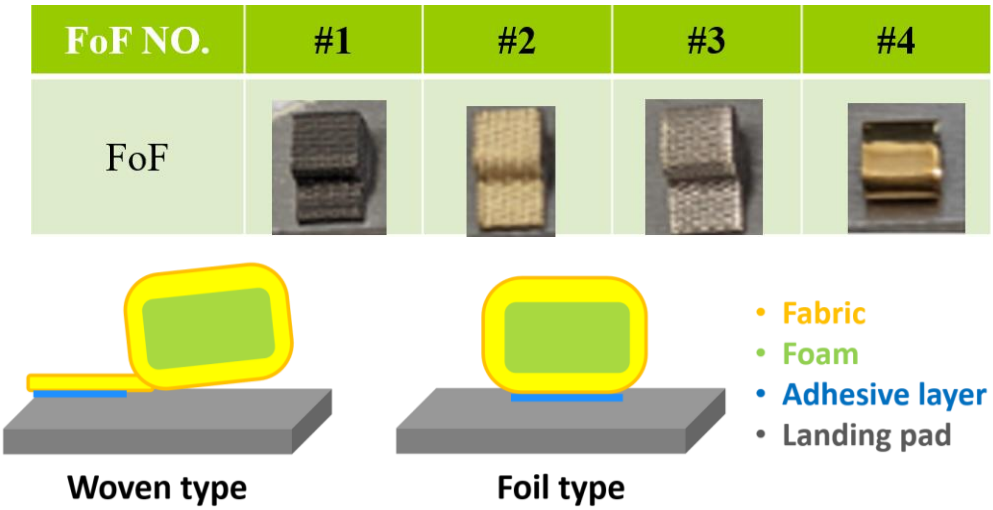

Figure 4.4 Different Types of FOF: the Electrically Conductive-Plated Fabric is Wrapped Over a Foam; the Adhesive Layer on The Bottom is used for Installment Purposes.

The measured and estimated PIM for FOF at 20 dBm input power is shown in Figure 4.5(a); The PIM is proportional to $log_{10}|a_3|$, as mentioned earlier. In addition, from Figure 4.5(b), notice that the PIM level does not always decrease with higher contact force, while the I-V based estimation can still reasonably capture the trend, primarily within 10 dB discrepancy. More than 500 cases were collected with different FOF types and contact forces, and the input power is swept among 10-20 dBm for each case.

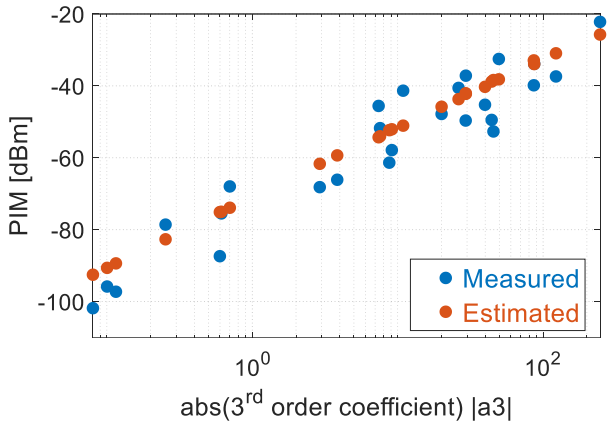

(a)

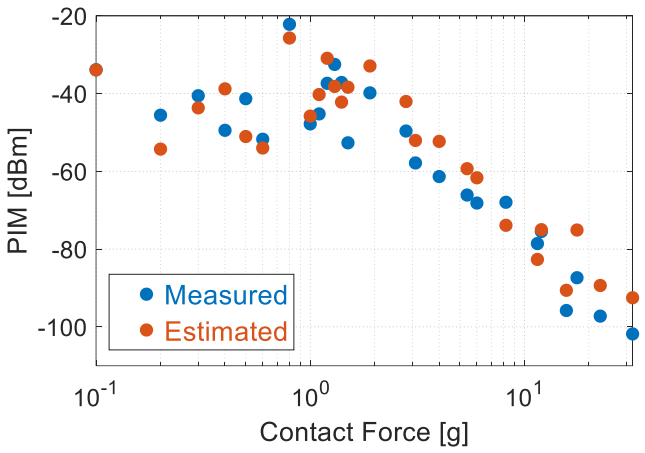

(b)

Figure 4.5 Measured Versus Estimated PIM for FOF #4 at 20 dBm Input Power: (a) PIM Versus Third Order Coefficient from the Fitted I-V Curve, (b) PIM at Various Contact Forces.

Figure 4.6 summarizes the discrepancy between the measurement and estimation. Ninety percent of the cases from woven-type FOF are captured within 10 dB discrepancy.

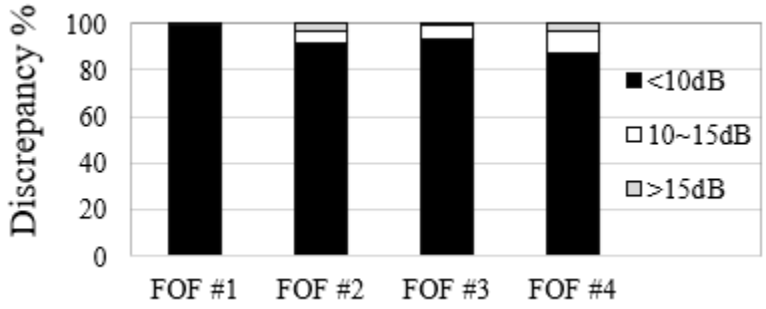

Figure 4.6 Discrepancy of Measured and Simulated PIM for Various Combinations of Landing Pad and FOF.

Several causes account for the discrepancies. First, the tiny contact area of spring contact, especially at loose contact force, makes it challenging to achieve an accurate PIM prediction. The smaller the contact area, the higher the nonlinear current density for a certain PIM level, resulting in unstable mechanical connection. Therefore, statistical analysis based on a large database is needed. Second, the imperfect I-V test – the current path of the static I-V test may be different from the RF current path. The pulsed I-V tests have potential to overcome the issue. Third, the I-V test itself may change the characteristics of the metallic contact, which is why the pre- and post-PIM need to be monitored to make sure the measured I-V can be correlated with the PIM. Besides, only the third order polynomial is applied for the I-V fitting, so numerical error exists. Though higher-order polynomial fit allows a better fitting, it increases the possibility to cause overfitting.

4.3. AGING TEST

Corrosion and oxidation on the surface of metals are among the major barriers in maintaining good metallic connections. The growth of the oxide layer varies depending on the specific metal type and the extent of environmental exposure. These unintentional barriers not only affect signal flow at RFs, but also potentially affect the current flow at a DC. An elevated TRH aging mechanism is considered to characterize the exposure of the FOF metallic contacts to the environment. Seventy-two hours of aging test is conducted using a temperature-humidity climate chamber. The impact of environmental aging on PIM, DC resistance and hardness of the metallic contacts are studied. Keeping the PIM measurement set-up, the same as the one used for validating the estimated PIM, a 4-wire measurement setup (Kelvin connection) adapted from [18] is used to understand the variation of the contact resistance at DC. The four wires are connected to the microstrips right next to the DUT and the resistance reading is obtained by a digital multimeter as shown in Figure 4.7 at various level of contact forces.

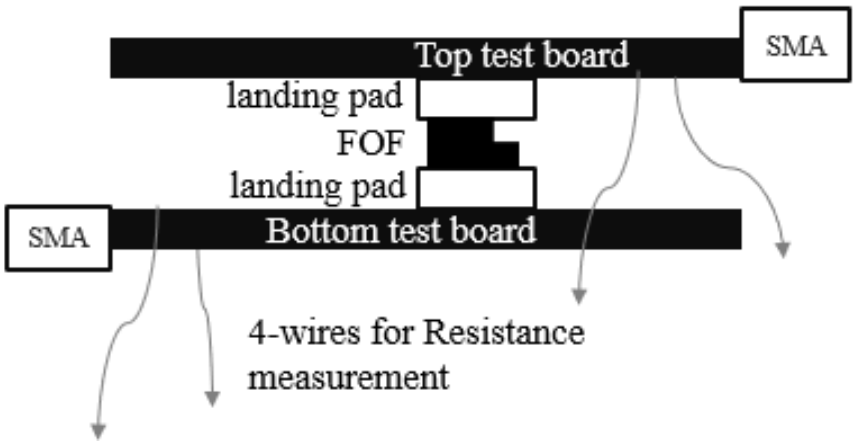

Figure 4.7 Test Set-Up DC Resistance (DCR) Measurement.

The conductive fabric of the FOF is produced by coating a nonconductive fabric with conductive material, using different coating processes [19]. The structure of the FOF is shown below in Figure 4.8.

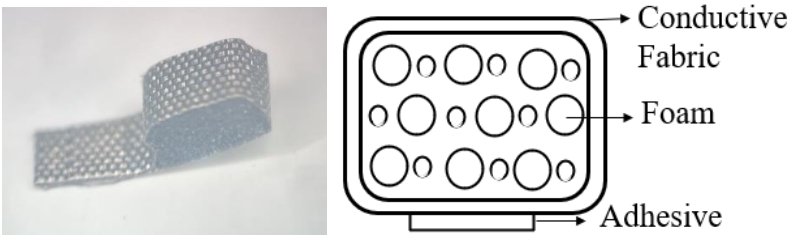

Figure 4.8 Fabric-Over-Foam (FOF) Material Structure used in Electronic Devices.

The elemental composition of the conductive surface can be obtained using energy dispersive spectroscopy (EDS) analysis. From an EDS analysis in Table 4.1, it has been found that Nickel is the base metal of the FOF type used throughout this paper. According to [20], Nickel plating is employed to increase physical qualities, such as wear resistance, heat resistance, or corrosion resistance. Nickel coatings play a crucial function in a variety of applications by enhancing corrosion resistance.

Table 4.1 Elemental Composition of the Conductive Fabric Surface from EDS Analysis.

Element	**Weight %**
C	7.51
N	1.25
O	4.26
Cl	1.48
Co	1.71
Ni	81.86
Pd	1.93
	100

4.3.1. Test Procedure. Two rounds of PIM and DC resistance data are taken before and after aging the samples to have a clear comparison of understanding the aging effect. A set of fresh nickel based FOF samples which have been fabricated recently are prepared to conduct this study. The PIM (IP3) levels sweeping the contact force are measured at 20 dBm input power to the metallic junction and the contact DC resistance is recorded from the digital multimeter at each corresponding contact force. The contact force is swept from zero (no contact) to 0.65 N (well-maintained contact) using a step motor. The maximum force is set to be not greater than 0.65 N to avoid over-compression. Figure 4.9 shows the PIM-Force and DCR-Force plots before the samples go under the aging test.

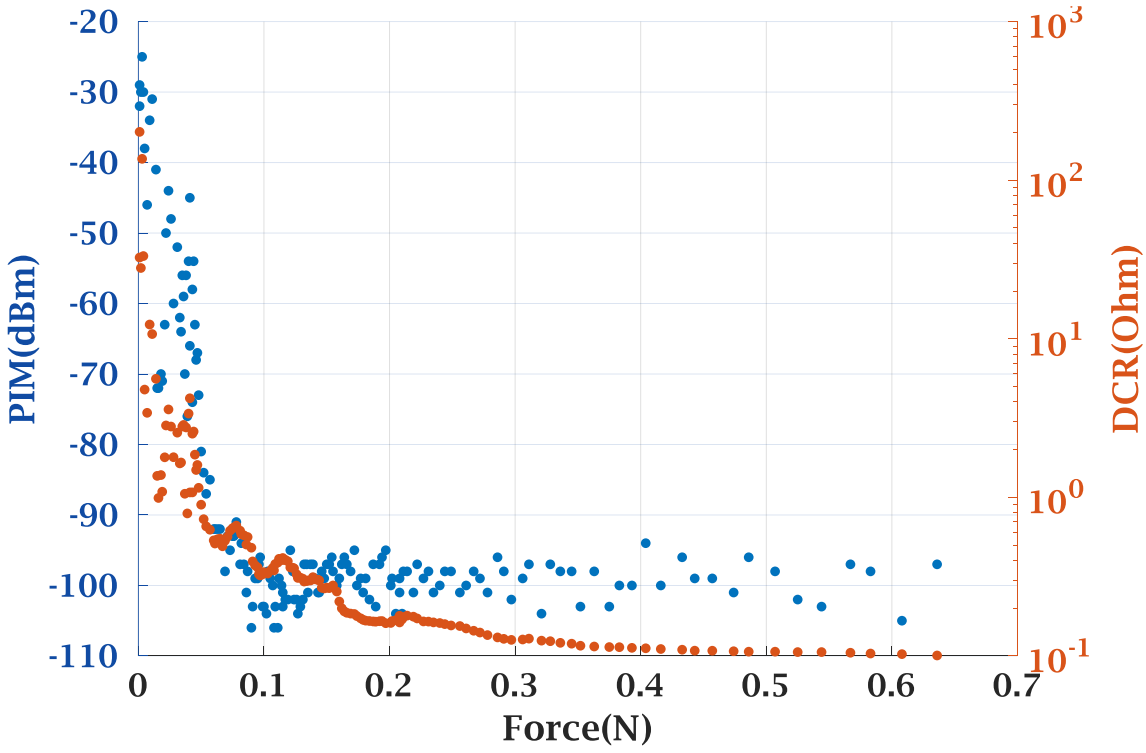

Figure 4.9 Fresh (Unaged) FOF Measurement Data: PIM-Force And DCR-Force.

In addition to the PIM and contact DC resistance, Force-step curve data are recorded to understand the change in flexibility of the FOF throughout aging. A Force-Step curve shows the amount of force needed to press the samples at a certain distance. This distance is the measured from the reference point (bare contact of the landing pad and the FOF) to the distance at higher contact force. As these samples are made up of foam between the conductive fabric, it is expected for a higher relative humidity to affect the hardness of the material.

After the PIM and DCR data are taken for the prepared set of fresh samples, the samples are placed in the climate chamber for accelerated aging. This study focuses only on the aging of the FOF material itself and the aging effect while the material is in contact with the metal chassis is not considered. The samples are placed on an acryl plate to avoid any changes resulting due to reactions if it was placed on a metallic surface. The test condition is set to be temperature of 65 ℃ and 90% RH (relative humidity). The samples are placed once the chamber is warmed up and been fixed to the above test condition. seventy-two hours (three days) of aging is implemented.

Having seventy-two hours of aging conducted, the test samples are taken out of the climate chamber and air blown for drying before conducting the PIM and DC resistance measurement again. Air blowing the material before conducting measurements allows removing the moisture effect due to the steam during the aging process in the climate chamber. No heat is applied while drying the sample to avoid an additional factor toward the recorded measurement data. The test procedure for conducting the measurement is shown in Figure 4.10 with a flow chart.

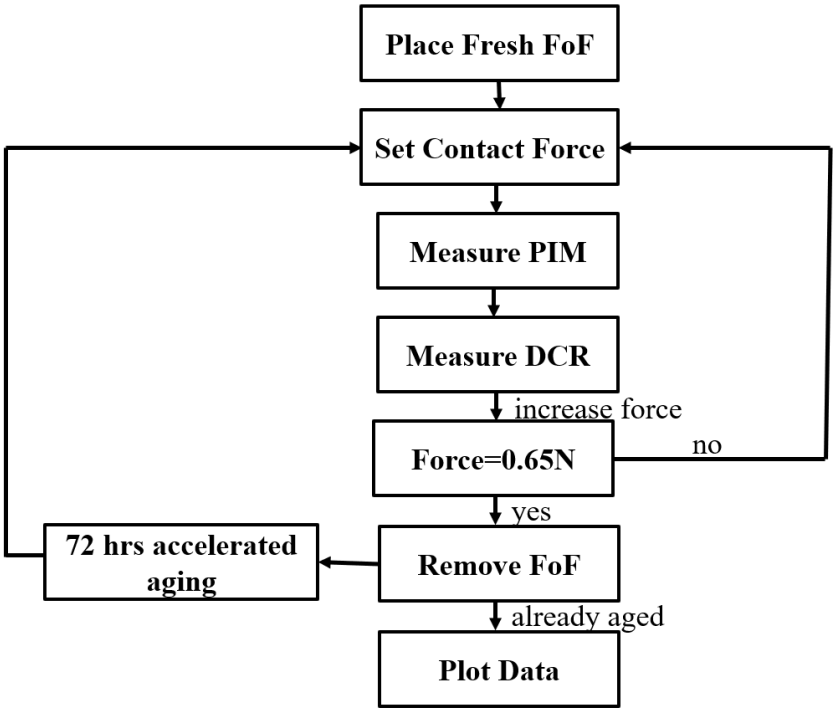

Figure 4.10 Flow Chart of the Aging Test.

4.3.2. Measurement and Data Analysis. Two types of data collection methods are implemented. The first one is to track the aging effect every twenty-four hours for three days, while the second one is to track the changes only once fully aged for seventy-two hours.

Although tracking the variation in PIM and DC resistance every 24 hours is expected to help to understand the whole aging process impact, it was found that the frequent assembly and removal of the FOF from the metal chassis reduces the contact strength of the adhesive. The spikes in PIM lever are observed at a higher contact force as shown in Figure 4.11(a). These higher-level IP3 values are caused due to the weak adhesive contact resulting in the tail part of the FOF forming a curvature and creating unintentional contact with the upper metal landing pad. An insulation tape (Kapton tape) is used to avoid

this unintentional contact and the samples are measured again. As shown in Figure 4.11(b), the results show no higher PIM spikes at a good contact region with the insulation tape as there is no more tail-upper landing pad unintentional contact.

The tail-upper landing pad contact is well demonstrated below in Figure 4.12. The left-hand side(a) shows fresh FOF with strong adhesive and the right-hand side(b) shows the unintentional contact after the adhesive got less sticky.

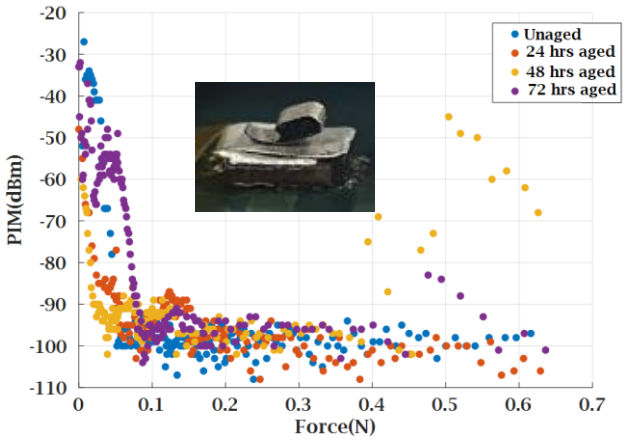

(a)

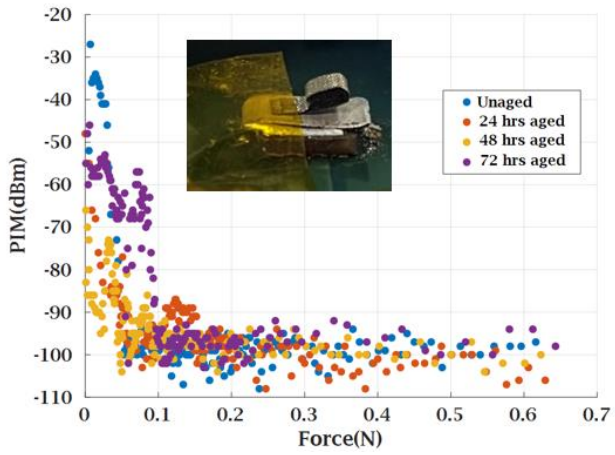

(b)

Figure 4.11 PIM Level across Various Contacts (a) FOF Curvature (b) Insulation (Kapton Tape) used to Avoid the Curvature Touching the Upper Landing Pad.

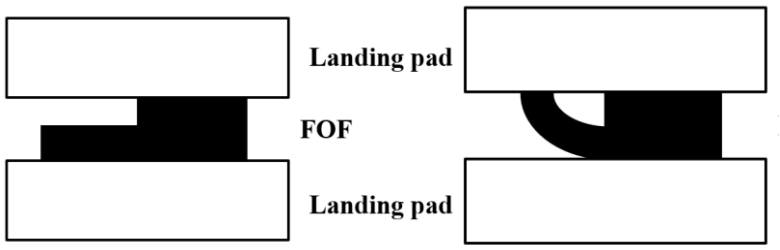

Figure 4.12 FOF-Landing Pad Contact: (a) Fresh FOF (b) Tail-Landing Pad Contact after Frequent Removal and Assembly.

In the second scenario, the FOF samples were kept continuously in the climate chamber for seventy-two hours. The PIM and DC resistance data measured from fourteen samples are plotted in Figure 4.13. The impact of the aging on the PIM level has been found to have little to no effect on some cases and the lowest PIM floor increment for the rest as shown in Figure 4.13 (a). Also, the tail-upper landing pad contact effect is still observed which indicates that the adhesive on the bottom surface of the FOF became less sticky resulting in a weaker contact. Figure 4.13 (b) shows the increase in DC resistance of the samples throughout aging for all the cases.

4.3.3. Static I-V based PIM Estimation after Aging. To demonstrate the fact that, only the RF signals being affected due to the unintentional discontinuity, a static I-V based PIM estimation is implemented to predict the level of the PIM. The estimation technique was implemented by gradually sweeping the current and obtaining a static I-V curve. The curve is then fitted, and the coefficients were extracted to calculate the corresponding PIM level. The method estimated the actual PIM level effectively before aging and did not capture the spikes after aging due to the additional current path from the unintentional tail-upper landing pad contact as shown in Figure 4.14.

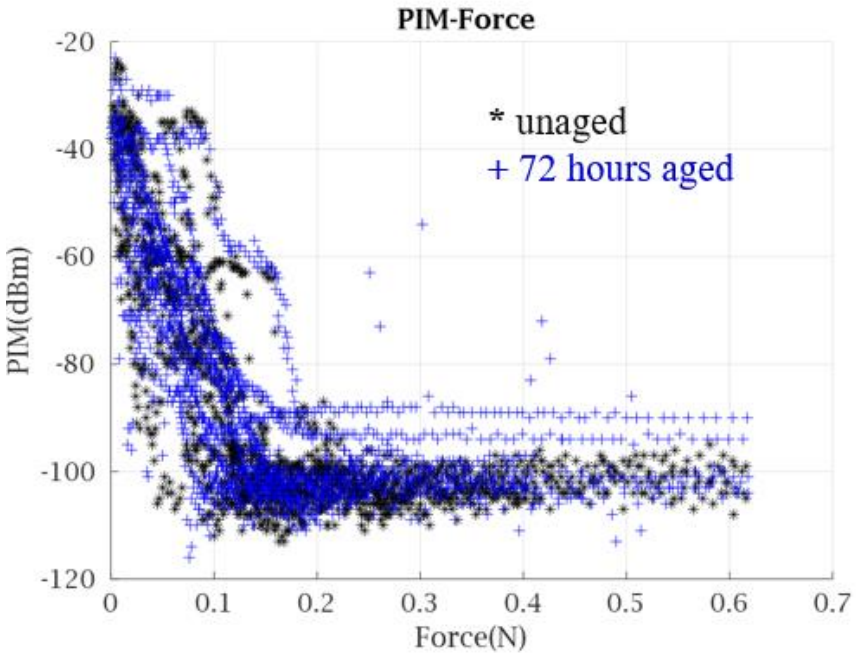

(a)

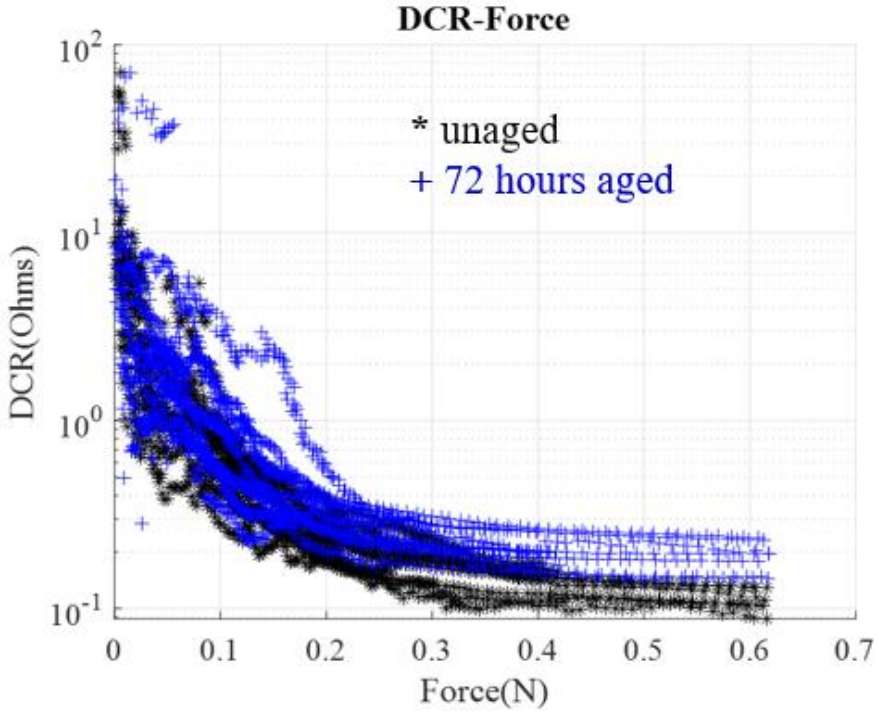

(b)

Figure 4.13 Fresh and Aged Data Comparison of Continuously Aged FOF for 72 Hours (a) PIM-Force (b) DCR-Force.

With the unintentional tail-landing pad contact, an additional current path was created which potentially affects signals as the desired frequency gets higher. This unintentional current path had an impact only on the RF signals and the DC resistance was not affected. DC measurements do not have the capability to capture multiple current paths and thus a static I-V based PIM evaluation cannot be implemented to estimate the PIM level for such cases.

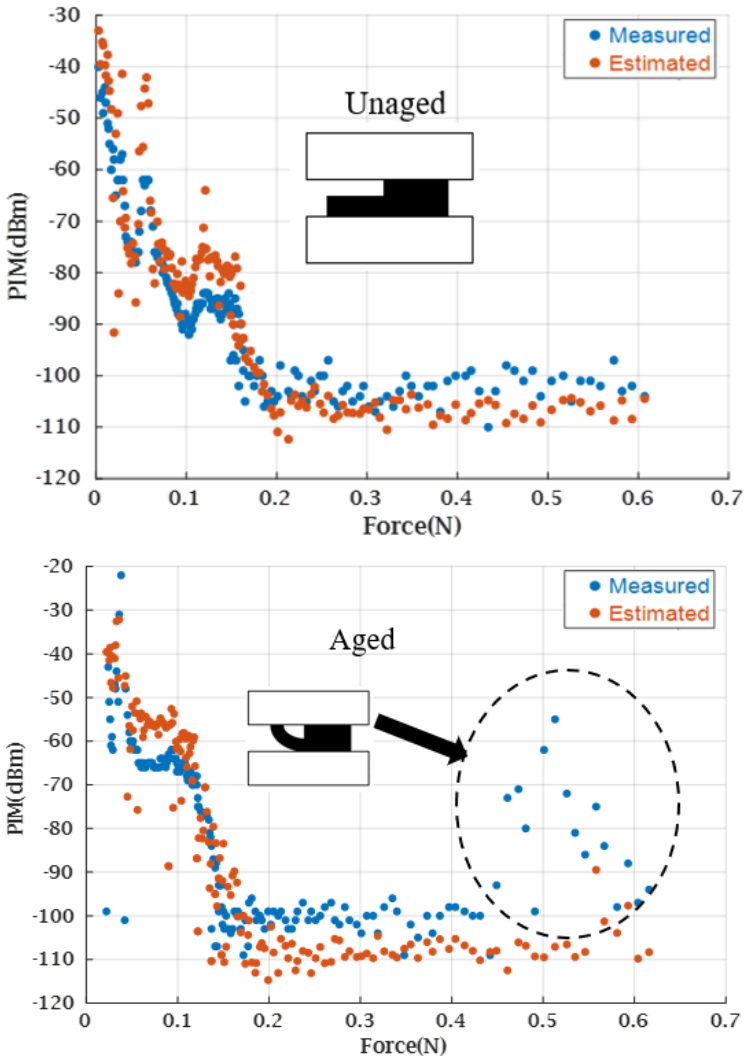

Figure 4.14 Static I-V Based PIM Estimation before and after Aging.

4.3.4. Surface and Material Composition Analysis. To further understand the changes in the contact DC resistance of the FOFs, microscopic images of the conductive fabric surface are taken using scanning electron microscopy (SEM). Figure 4.15 Shows these microscopic images for unaged and aged samples. There is no significant change on the surface of the material observed after the seventy-two hours of elevated TRH aging process.

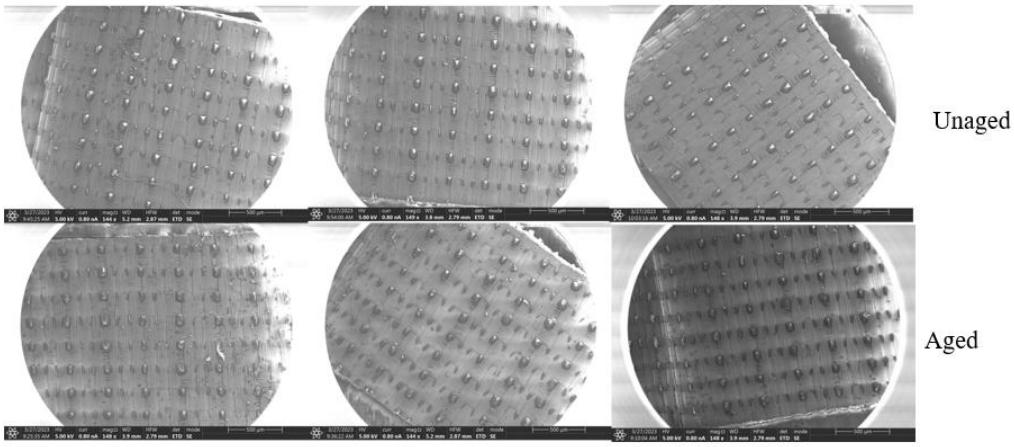

Figure 4.15 Microscopic Images for the Conductive Fabric Surface of FOF using Scanning Electron Microscopy (SEM) for Unaged and Aged Samples.

In addition to the SEM, an EDS analysis is conducted to see the variation in elemental composition of the surface. The chemical reaction between elements found in the environment specifically oxygen and the polymers used in making FOF surface would result in an oxide formation. Thus, the base metal Nickel and the oxygen compositions are compared before and after aging in Figure 4.16.

After the FOF went through elevated TRH environmental aging, a growth in oxygen composition is observed indicating an oxide layer formation on the surface of the

FOF. However, actual oxide layer formed on the surface highly depends on the reaction between polymers of the FOF with environmental oxygen [21]. The DC resistance increment observed during measurement is expected to be due to this oxide formation.

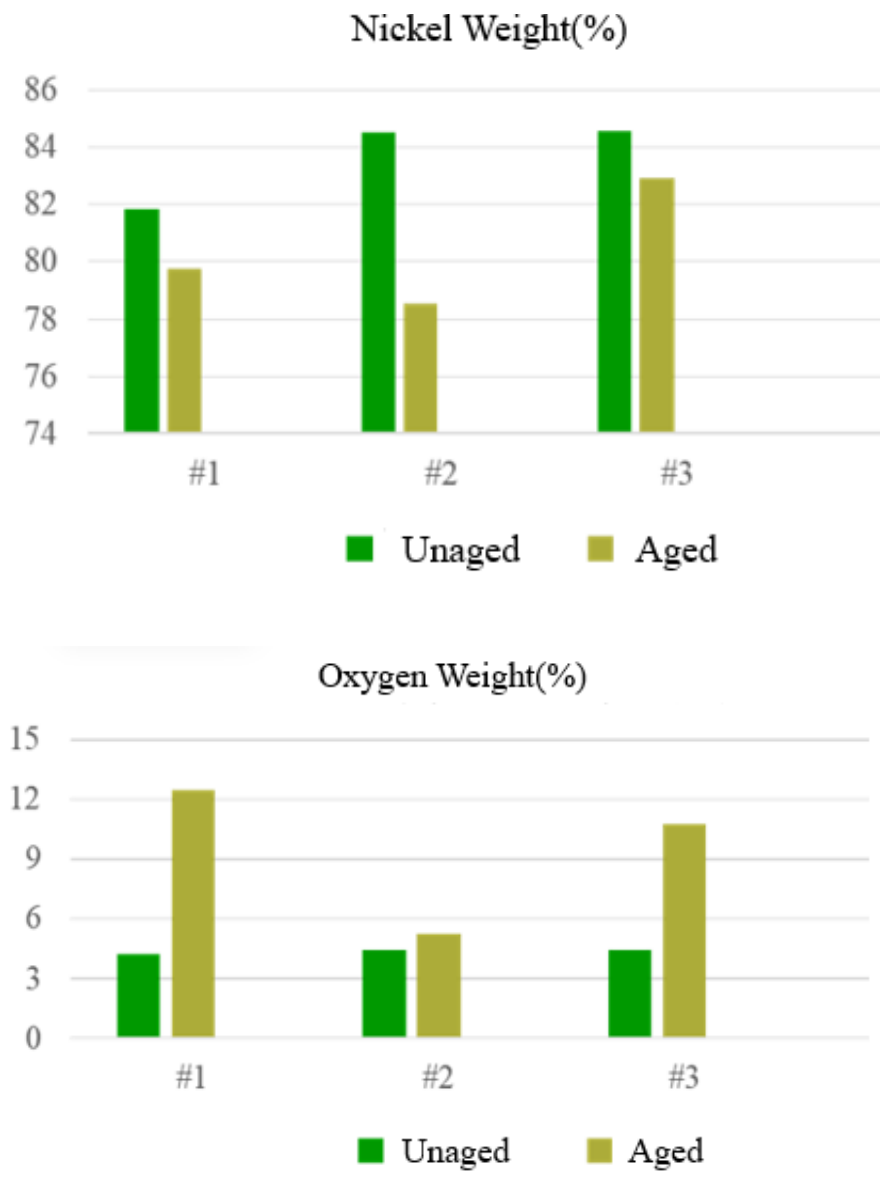

Figure 4.16 Elemental Composition of the Conductive Surface of the FOF using Energy Dispersive Spectroscopy (EDS) Analysis.

The next data shown in Figure 4.17 is the force-step curve to understand the change in the hardness of the FOF throughout the aging process. The results show that the FOFs become softer after aging.

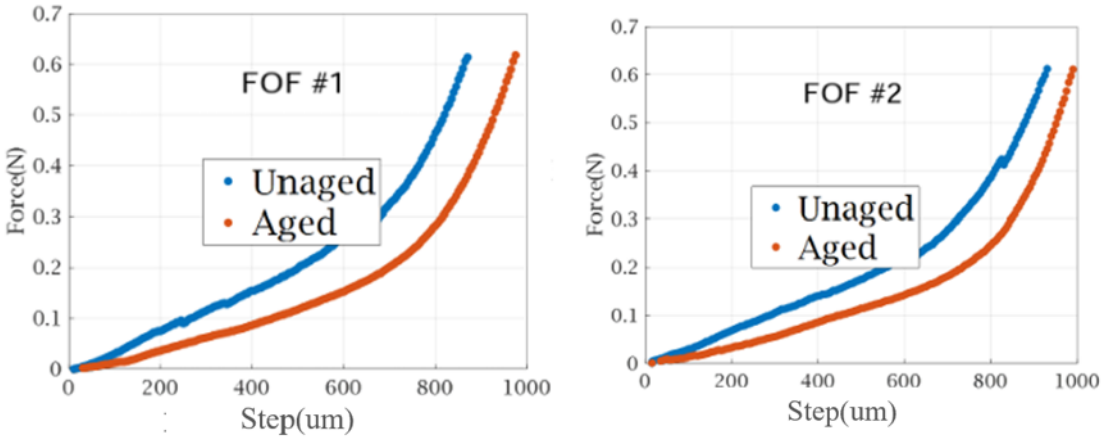

Figure 4.17 Force-Step Curve of FOF before and after Aging.

5. CONCLUSIONS AND FUTURE WORKS

An I-V based PIM estimation method is proposed to estimate the PIM in spring and FOF contacts. The overall discrepancy of PIM between measurement and I-V based estimation is within 20 dB in 85% cases of spring contacts and within 10 dB in 90% cases of FOF contacts. It was observed that the higher nonlinearity of I-V shows, the higher the PIM levels are observed. Considering the complexity and expensive cost of PIM setup, a simple way to identify the possible high PIM risk is needed. The I-V test provides the way with easier implementation in massive factory tests. Correspondingly, the spring clip and FOF suppliers can have a simpler and inexpensive way to try various combinations of material, surface treatment, and product shape to optimize the design.

An elevated TRH environmental aging test is ALSO conducted to understand the variation in PIM and contact DC resistance to characterize an aging of FOFs. The measured results demonstrate that PIM level variation could happen due to weaken adhesive contact and a DC resistance increment due to an oxide formation on the surface of FOF throughout aging.

Other higher order intermodulation products can be studied in the future for systems with higher input power since the PIM level gets higher as the input power increases.

BIBLOGRAPHY

[1] J. G. de la Rosa, J. M. Rebollar, E. L. M. Ramírez, and D. P. Escalona, "Measurement System for Intermodulation Distortion in RF Components," in IEEE Transactions on Instrumentation and Measurement, vol. 69, no. 7, pp. 4773-4782, July 2020, doi: 10.1109/TIM.2019.2944913.

[2] F. Gardiol, C. Di Paolo, and P. Peroni, "Effects of passive intermodulation in wireless systems: models and measurements," in IEEE Transactions on Instrumentation and Measurement, vol. 53, no. 3, pp. 890-896, June 2004, doi: 10.1109/TIM.2004.825642.

[3] "Passive Intermodulation (PIM) in RF Systems," Norsat International Inc., [Online]. Available: https://www.norsat.com/resources/blog/what-is-passive-intermodulation-pim/.

[4] L. Pajusco, S. C. Pavone, A. M. Pasian, and C. B. Soares, "Passive Intermodulation in GSM Networks: Measurements and Modeling," in IEEE Transactions on Instrumentation and Measurement, vol. 53, no. 3, pp. 869-874, June 2004, doi: 10.1109/TIM.2004.825644.

[5] D. Konstantinov, M. I. Petrov, V. S. Petrova, and K. I. Atanasov, "PIM Simulation and Estimation in Mobile Communication Systems," in 2018 41st International Spring Seminar on Electronics Technology (ISSE), Sofia, 2018, pp. 1-5. doi: 10.1109/ISSE.2018.8443852.

[6] G. Acosta-Valdés, M. Englund, and A. C. M. Castro, "Measurement and estimation of PIM in RF components for cellular communications systems," in IEEE Transactions on Instrumentation and Measurement, vol. 68, no. 10, pp. 4031-4039, Oct. 2019. doi: 10.1109/TIM.2018.2877909.

[7] K. Tang, F. Wang, K. Bai, W. Li, and H. Zhang, "Measurement and analysis of passive intermodulation in RF transmission lines and antennas," in IEEE Transactions on Instrumentation and Measurement, vol. 70, pp. 1-11, 2021. doi: 10.1109/TIM.2021.3079136.

[8] K. Wu, H. Jin, and W. Xia, "A Novel PIM Estimation Method for Troubleshooting in Mobile Communication System," in 2019 IEEE 89th Vehicular Technology Conference (VTC2019-Spring), Kuala Lumpur, Malaysia, 2019, pp. 1-5. doi: 10.1109/VTCSpring.2019.8746674.

[9] International Electrotechnical Commission (IEC), "IEC 62037: Passive RF and microwave devices, intermodulation level measurement," 2nd ed., Geneva, Switzerland, 2020.

[10] Q. Jin, J. Gao, L. Bi and Y. Zhou, "The Impact of Contact Pressure on Passive Intermodulation in Coaxial Connectors," in IEEE Microwave and Wireless Components Letters, vol. 30, no. 2, pp. 177-180, Feb. 2020, doi: 10.1109/LMWC.2019.2957983.

[11] J. Henrie, A. Christianson and W. J. Chappell, "Prediction of Passive Intermodulation From Coaxial Connectors in Microwave Networks," in IEEE Transactions on Microwave Theory and Techniques, vol. 56, no. 1, pp. 209-216, Jan. 2008, doi: 10.1109/TMTT.2007.912166.

[12] Q. Jin, J. Gao, G. Xie, G. T. Flowers and R. Ji, "A study of the passive intermodulation induced by nonlinear characteristics of RF connectors," 2016 IEEE 62nd Holm Conference on Electrical Contacts (Holm), Clearwater Beach, FL, USA, 2016, pp. 1-8, doi: 10.1109/HOLM.2016.7779999.

[13] P. L. Lui, "Passive intermodulation interference in communication systems," *Electronics and Communication Engineering Journal*, vol. 2, no. 3, p. 109, June 1990

[14] P.-L. Lui, "A Study of Intermodulation Interference Due to Non-linearities in Metallic Structures," Ph.D dissertation at the University of Kent, Canterbury p. 215, 1990.

[15] J. J. Henrie, A. J. Christianson and W. J. Chappell, "Linear–Nonlinear Interaction and Passive Intermodulation Distortion," in IEEE Transactions on Microwave Theory and Techniques, vol. 58, no. 5, pp. 1230-1237, May 2010, doi: 10.1109/TMTT.2010.2045527

[16] X. Zhao et al., "Analytic Passive Intermodulation Model for Flange Connection Based on Metallic Contact Nonlinearity Approximation," in IEEE Transactions on Microwave Theory and Techniques, vol. 65, no. 7, pp. 2279-2287, July 2017, doi: 10.1109/TMTT.2017.2668402.

[17] S. Xia et al., "Practical Fixture Design for Passive Intermodulation Tests for Flexible Metallic Contacts," 2022 IEEE International Symposium on Electromagnetic Compatibility & Signal/Power Integrity (EMCSI), Spokane, WA, USA, 2022, pp. 17-22, doi: 10.1109/EMCSI39492.2022.9889578.

[18] S. Xia et al., "Gassian Process Regression Analysis of Passive Intermodulation Level and DCR for Spring Contacts," 2021 IEEE International Joint EMC/SI/PI and EMC Europe Symposium, Raleigh, NC, USA, 2021, pp. 935-939, doi: 10.1109/EMC/SI/PI/EMCEurope52599.2021.9559359.

[19] R. R. Bonaldi, "12a Electronics used in high-performance apparel" in *High-Performance Apparel* Woodhead publishing, Sawaston, UK. 2018

[20] Nickel plating handbook, 1st ed. The Nickel Institute, Durham, North Carolina, U.S.A.,2013

[21] Choi SB. et al, “Role of Oxygen in the Ti_3AlC_2 MAX Phase in the Oxide Formation and Conductivity of Ti_3C_2-Based MXene Nanosheets”, *ACS Appl Mater Interfaces.* 2023 Feb 15;15(6):8393-8405

VITA

Kalkidan Anjajo holds a Bachelor of Science degree in Electronic Information Engineering from UESTC (University of Electronic Science and Technology of China), earned in July 2021. Additionally, she obtained a Master of Science degree in Electrical Engineering in July 2023 from Missouri University of Science and Technology (MST). With a strong educational background in engineering, Kalkidan has developed expertise in areas such as signal and power integrity, RF interference, and electromagnetic compatibility. Her academic journey has equipped her with a solid foundation in technical skills and problem-solving abilities. She is highly motivated and dedicated to applying her knowledge and skills to contribute to the field of electrical engineering.